Hindawi
Advances in Civil Engineering
Volume 2023, Article ID 5577851, 18 pages
https://doi.org/10.1155/2023/5577851

Research Article

Enhancing Understanding of Hydrologic Processes in the Shafe Watershed, Ethiopia

Zerihun Makayno Mada[1] and Abera Shigute Nannawo[2]

[1]*Faculty of Hydraulics and Water Resources Engineering, Arba Minch Water Technology Institute, Arba Minch University, P.O. Box 21, Arba Minch, Ethiopia*
[2]*Faculty of Water Resources and Irrigation Engineering, Arba Minch Water Technology Institute, Arba Minch University, P.O. Box 21, Arba Minch, Ethiopia*

Correspondence should be addressed to Abera Shigute Nannawo; aberashigute@gmail.com

Received 7 September 2023; Revised 31 October 2023; Accepted 20 November 2023; Published 16 December 2023

Academic Editor: Rafael J. Bergillos

Research on the combined impact of watershed attributes on streamflow is crucial in water resources planning and management, particularly due to the strong link between landscape modification and watershed attributes. However, identifying critical watershed attributes remains a challenge. This study focuses on investigating the impact of watershed attributes on streamflow in the Hare catchment of Ethiopia's rift valley lakes basin. The Soil and Water Assessment Tool (SWAT) rainfall–runoff model was used, calibrated, and validated against observed discharge data to identify remedial measures for streamflow generation. The model's performance was evaluated using criteria such as R^2, NSE, PBIAS, and RSR, which yielded satisfactory values. The study found significant changes in land cover, with forest and shrub land declining and agricultural land expanding. Comparing mean annual streamflow between 1998, 2009, and 2021, streamflow at 2021 land use and land cover increased by 13.03% compared to 2009, which had already increased by 16.05% compared to 1998. The study also examined the impact of climate variations by manipulating meteorological data length and average slope. Overall, this study provides valuable insights into the relationship between watershed attributes and streamflow, emphasizing the importance of considering land cover changes and climate variations for effective water resource management in the Hare catchment.

1. Introduction

In Ethiopia, poor cultivation practices, and inadequate land and water resource systems, leading to increased sediment transport and soil erosion, and deterioration of water resources in both quality and quantity [1, 2]. The expansion of urban areas and agricultural land, and deforestation are the governing factors for temporal and spatial changes in land use and land cover (LULC), which has impacts on the sectors like hydropower, irrigation, and water supply [3–6]. Many basins in developing economies are deteriorating due to rising populations and excessive use of natural resources [7–9].

Land and water are crucial resources for social existence, and influence the persistence and degradation of watersheds [10]. These hydrologic responses are linked to variations in infiltration and evapotranspiration rates, which result in seasonal and long-term river discharge variability [11]. A decline in vegetation cover and subsequent soil degradation can also cause many of the threats associated with water-flow extremes peak and base flow [12]. Physical catchment characteristics (PCCs) have significant influence on water budget elements such as infiltration, interception, surface and subsurface flow. and potential evapotranspiration.

Watershed attributes can aid forest management and/or policy by indicating where forestry efforts would best be focused. The effects of forestry activities on water yield are different in watersheds, so watershed features can be used to describe the watershed's appropriateness or unsuitability for water production, as well as where and how much forestry should be done [4, 11]. The spatial dynamics of the hydrologic cycle are directly related to hydrologic modeling and water resources management studies [13, 14]. The hydrologic cycle,

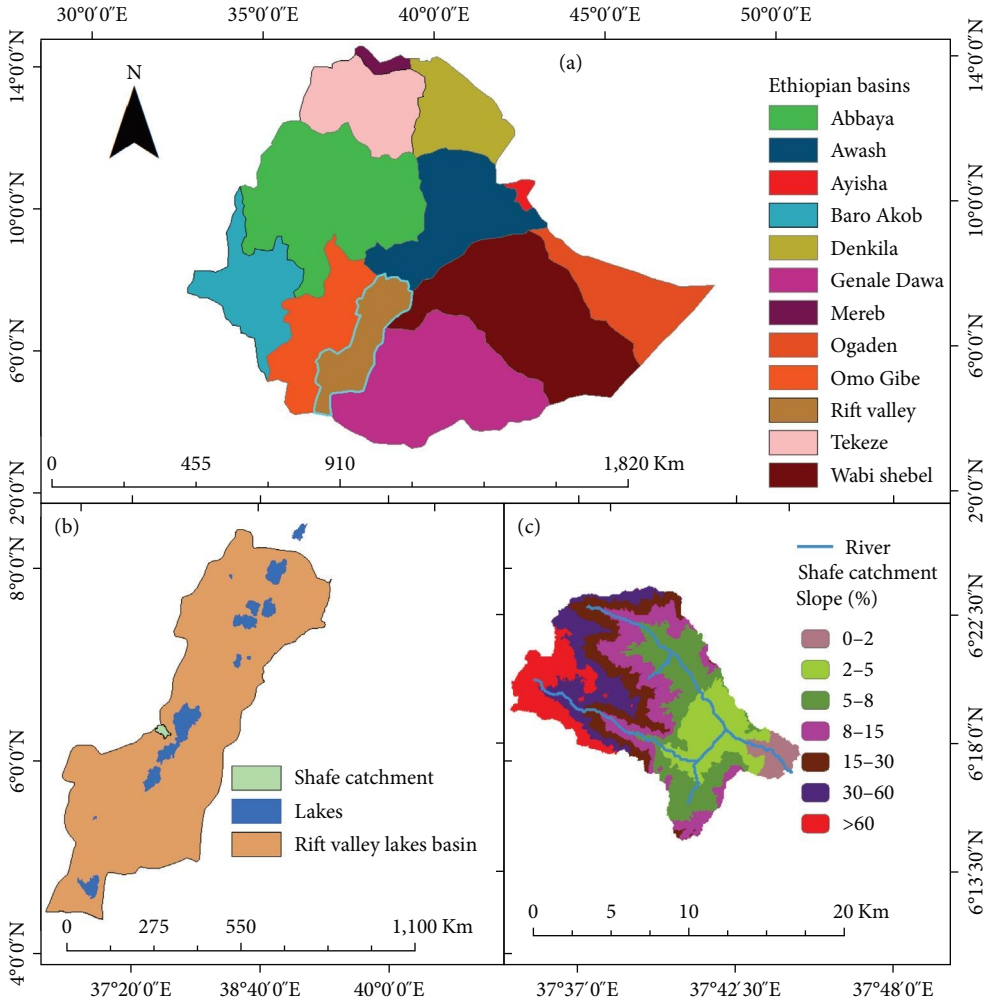

Figure 1: Study area showing: (a) Ethiopian basin, (b) Rift Valley Lakes Basin, and (c) Shafe catchment slopes by class.

which involves the continual movement of water on, above, and below the earth's surface, is influenced by many variables, including climate change, LULC, slope characteristics, and river shape [15, 16]. Short-term hydrologic fluctuations are likely to be caused by topography and soil characteristics, while long-term developments like urbanization and deforestation lower evapotranspiration and water recycling, which can lead to a decrease in rainfall.

LULC are major variables in most hydrological models at all catchment scales. Changing forest to agricultural land or constructed areas has a significant impact on runoff, groundwater recharge, erosion, and sediment transport [4, 11]. Because LULC has such a significant impact on water quality and quantity, it is critical to understand how it, hydrology, and water resource management work together [17, 18].

LULC practices throughout a catchment are the major factor controlling flow and water quality. Settlements, firewood harvesting, agricultural expansion, and charcoal production have cleared many mountains and shorelines, as reported widely. Watershed management is one method of the conserving healthy, productive rivers. The aim of this study was to investigate the impact of various watershed attributes on streamflow in the Shafe catchment, in the Rift Valley Lakes Basin, Ethiopia. The significant LULC changes in the watershed were compared with their individual influences on streamflow, and potential corrective actions determined.

2. Materials and Methods

2.1. The Study Area. The Shafe catchment is in the Abaya–Chamo subbasin of the Rift Valley Lakes Basin, on the edge of the Great Rift Valley, and drains into Lake Abaya (Figure 1). The 23.8-km long watershed covers about 144 km^2, and lies between 6°15′ and 6°25′N, and 37°35′ and 37°45′E. Its altitude ranges from 1,259 to 3,056 m above mean sea level. According to Roth et al. [19] (Figure 1 and Table 1), the terrain slope was categorized, with the majority of it falling into the extremely steep (33.9%) and steep (33.7%) categories. Only roughly 4.2% and 2.4% of the area are classified as gently sloping or sloping, respectively, with 0.43% of the area being flat near Abaya Lake.

2.2. Climate. The catchment climate varies from tropical to alpine. The intertropical convergence zone (ITCZ) governs

Table 1: Slope classifications (based on FAO, 1985).

No.	Slope (%)	Classification
1	0–2	Flat
2	2–5	Gentle slope
3	5–8	Sloping
4	8–15	Moderately steep
5	15–30	Steep
6	30–60	Very steep
7	>60	Extremely steep

Table 2: Shafe catchment climate zones—Ethiopian classifications based on elevation.

Altitude range (m)	Zone	Covered (%)
0–500	Hot or arid	0
500–1,500	Semiarid	3.5
1,500.1–2,500	Semihumid	71
2,500.1–3,000	Cold humid	25
>3,000	Moist mild	0.2

the bimodal rainfall system, carrying humid winds from the Indian Ocean. Rainfall distribution in the area is also affected by altitude. There are four traditional climate zones in the Shafe catchment. About 70% and 25%, respectively, of the catchment are characterized as semihumid and cold humid (Table 2).

The bimodal rainfall distribution incorporates an extended rainy season from early March to late June, with maximum rainfall occurring around April, and a shorter one from mid-August to mid-October. The other months are generally dry, with intermittent rainfall. The minimum monthly rainfall is recorded in January as can be seen in Figure 2.

2.3. Temperature. The study area's long-term temperature is based solely on data from Arba Minch station (from 1995 to 2021). Figure 3 shows that the highest temperature is recorded between February and April, the lowest between May and September.

2.4. Data Collection and Analysis. In order to enhance the quality of data collected from Ethiopian Ministry of Water and Energy, missing data were estimated, and the data's availability, consistency, and homogeneity were checked. Meteorological data were obtained from the National Meteorological Agency of Ethiopia (NMAE) [20]. The study area's proximity led to the selection of Arba Minch, Chencha, and Mirab Abaya climatic data stations. Unfortunately, the time-series data are insufficient, inconsistent, and include several breaks. A record's consistency may be affected by data missing for a variety of causes, but data from neighboring stations can be used to make estimates of the missing data. Various techniques have been used to approximate missing rainfall data, but the inverse distance method—Equation (1)—is the most accepted in scientific investigation and was used in this study as follows:

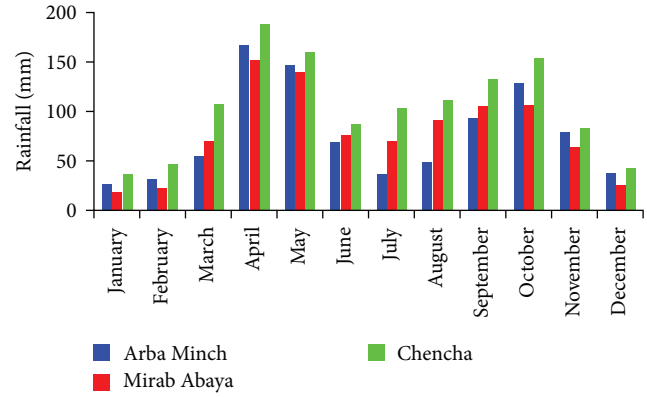

Figure 2: Mean monthly rainfall, Shafe subcatchments (1995–2021).

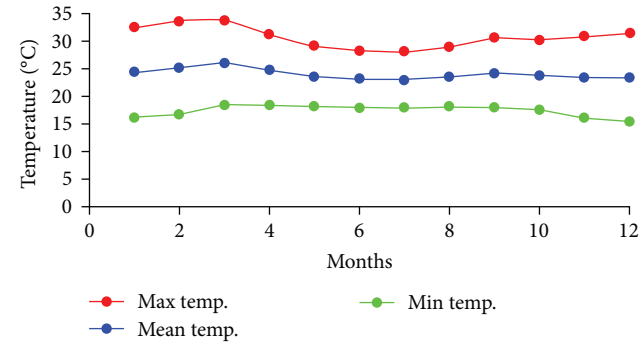

Figure 3: Maximum, minimum, and average monthly temperature (°C) at Arba Minch station (1995–2021).

$$P_X = \frac{\sum_{i=1}^{n} P_i}{\sum_{i=1}^{n} W_i}, \tag{1}$$

where W_i is calculated using Equations (2) and ((3)) as follows:

$$w_i = \frac{1}{D^2}, \tag{2}$$

$$D^2 = \Delta X^2 + \Delta Y^2. \tag{3}$$

In Equations (1)–((3)), P_x = missing precipitation item; P_i = precipitations at the index stations, W_i = station weighting, and D^2 = station distance from that with missing data.

2.5. LULC Evaluation and Satellite Image Classification. Remote sensing techniques were used to detect general LULC patterns from 1998 to 2021. USGS satellite images were downloaded and the study period divided into three sets: 1998, 2009, and the period 2010–2021. A false-color composite (RGB) image was created from bands 1, 2, and 3 as the background for the supervised classification of all 1998, 2009, and 2021 images (Figure 4). ArcGIS was used to prepare the LULC data for SWAT input, to enable the detection of changes [1, 21].

"Supervised-classification" uses a chosen raster and coordinates from actual LUs to color-code different LULC

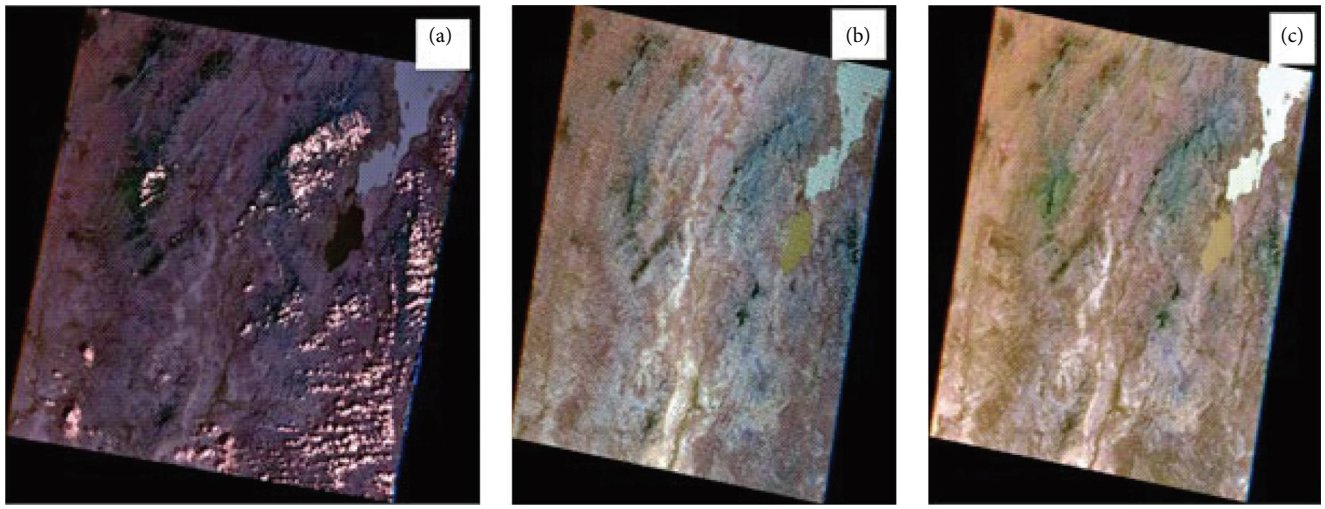

Figure 4: Landsat imagery 1998 (a), 2009 (b), and 2021 (c).

Table 3: Main LULCs.

Major land cover	Description
Agricultural land	Annual and perennial crop cultivation; scattered rural settlements with some pasture and plantations around them
Forest	Trees and other plants in a large, densely wooded area that can be evergreen, deciduous or mixed
Shrubland	Sparsely located trees with brush and shrub types, including bushes and woodland
Grassland	Land where the potential natural vegetation is predominantly grasses and grass-like plants

groups. The method enabled existing land uses to be grouped into four main categories, and the multilabel classification algorithm was used to derive their signatures. Four land classes were created: agricultural land, grassland, forest, and shrub land (Table 3).

2.6. Streamflow Prediction in the Ungauged Shafe Catchment. Streamflow prediction in ungauged basins plays key role for water resources planning and environmental managements [22, 23]. Reliable streamflow data contains valuable information for various purposes, including environmental impact assessment, estimation of hydrologic extremes, low-flow estimation, design of hydraulic structures, and water resources planning [24]. The International Association of Hydrological Science gave significant attention to the prediction of streamflow in ungauged basins from gauged basins during the period of 2003–2012 [25]. Therefore, generating streamflow data in ungauged catchments are a fundamental task before conducting any environmental impact assessment [26].

Predicting streamflow in ungauged basins is one of the major concerns in water resources studies, especially in regions with high-spatial variability of hydrological environment. Because several parts of the world streamflow measuring networks are decreasing due to the impacts of climate and anthropogenic issues [27]. Several researchers [28–30] have suggested that regionalization is the most common way to address the problems of ungauged catchments by transferring the information from gauged to receivers because it considers hydrological process, integrates different catchment characteristics, and relatively better estimation.

The prediction of streamflow in ungauged basins is a major concern in water resources studies, particularly in regions with high-spatial variability of hydrological conditions. This is due to the decline in streamflow measurement networks in several parts of the world as a result of climate change and human activities [31]. Recently, regionalization has been conducted and suggested by several researchers for instance [32] conducted excess streamflow prediction in the Sebou basin for an interbasin water transfer, Purvis and Dinar [33] did streamflow prediction in ungauged catchments for an interbasin water transfer sustainable policy intervention to alleviate water scarcity. Also, Rientjes et al. [34] performed regionalization for hydrological balance in Upper Blue Nile basin, Ethiopia. Different methods have been developed for predicting streamflow data in ungauged catchments. However, the major one being used in this study is regional model method through rainfall–runoff modeling tools and physical catchments characteristics [35, 36].

Streamflow generation in the Abaya Chamo lakes subbasin is influenced by various catchment characteristics. In this study, a 30×30 m resolution digital elevation model (DEM) was utilized to delineate catchments within the study area. Four major categories of PCCs were considered, including geography and physiography (e.g., area, perimeter, basin shape, average slope, elongation ratio, and longest flow path), geology and soil (e.g., drainage density, bifurcation ratio, and percentage cover of different soil types), land use land cover (LULC) (e.g., percentage cover of different LULC types), and climate (e.g., annual average rainfall and average annual evapotranspiration).

Hydrological regionalization involves transferring hydrological information from gauged basins to ungauged basins or

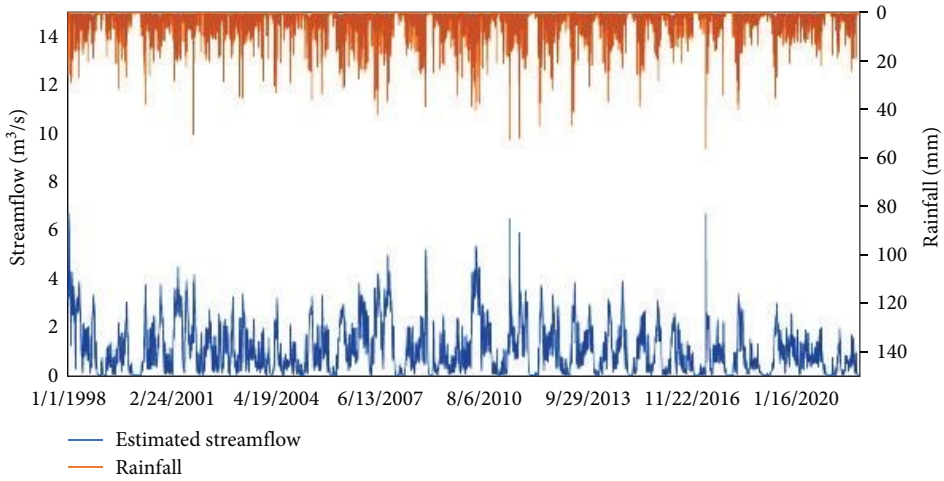

FIGURE 5: Estimated streamflow in the ungauged Shafe catchment.

transferring optimized model parameters from donor catchments to target catchments [37]. In this study, multiple regression-based hydrological regionalization was selected due to its widespread usage and better results [29, 38]. This technique utilizes model parameters as dependent variables and physical catchment attributes as independent variables.

For regionalization in the Abaya Chamo lakes subbasin, four gauged catchments (Bilate, Bedessa, Hare, and Gidabo) were used. These catchments are neighboring watersheds to the Shafe catchment, sharing similar geographical landscapes and draining into Lake Abaya. They exhibited good performance, with the objective function of relative volume error (RVE) ranging from +10% to −10% and the Nash–Sutcliffe efficiency (NSE) value greater than or equal to 0.60. The HBV–IHMS hydrologic model was calibrated using these catchments, and their model parameters and PCCs were intercorrelated to determine the parameters for the ungauged Shafe catchment. The multiple regression method, implemented in ArcGIS, was used to establish the relationship between PCCs and model parameters.

Correlation analysis was conducted between each model parameter and all PCCs. The PCCs exhibiting a higher correlation with the model parameters were selected as regression inputs. The PCC with the highest correlation was entered first, and its statistical significance was assessed to determine its suitability as a potential candidate for the regional model. The collinearity of the PCCs was evaluated based on the statistical significance (p-values ≤ 0.1 for a 95% confidence interval) and coefficient of determination ($R^2 \geq 0.80$).

Once the first PCC was selected based on its statistical significance, the second PCC with the next highest correlation was included in the multiple regression. The optimized model parameters and PCCs of the gauged catchments were used to establish these correlations. The development of the regional model involved using the multiple linear regression method, with the PCCs as independent variables and the model parameters as dependent variables. Stepwise multiple regression, performed using Excel data analysis, was employed to select the best independent variables. The following Equation (4) provides a brief description as:

$$M = \beta 0 + \beta 1 \times P1 + \beta 2 \times P2 + \ldots\ldots \beta n \times Pn, \tag{4}$$

where, $\beta 1$, $\beta 2$, and βn are the coefficients of regressions, $P1$, $P2$, and Pn are independent variable (PCCs), M is dependent variable (MPs), and βo is intercepting of regression line.

Both forward selection and backward elimination were used in multiple regression analysis for this study, and the sample multiple regression equation between model parameters and PCCs. Figure 5 shows transferred model parameters, simulated flow and the Shafe catchment HBV–IHMS transferred model parameters better estimated streamflow, because in the high-rain reasons high-streamflow volume and in low-rain seasons minimum flow is generated.

Alfa $= -0.34 + 1.61 \times$ drainage density $+ 0.01 \times$ Solonchak soil $+ 0.039 \times$ barren land

Beta $= -1.09 + 0.56 \times$ bifurcation ratio $- 0.02 \times$ Xerosol soil $+ 0.74 \times$ elongation ratio $- 0.23 \times$ forestland

Perc $= -3.25 - 0.61 \times$ Leptosol soil $- 0.01 \times$ basin shape $+ 0.005 \times$ annual potential evapotranspiration.

3. Trend Analysis

3.1. Mann–Kendall (MK) Test. The MK test is a nonparametric trend analysis test that uses Kendall's tau statistic [39–42]. The test was first initiated by Mann (1945). In this study, the MK test statistic has been derived using Sen's slope estimator to indicate the slopes' outcomes [41, 43–46] Equation (5). However, it only considers the slope's sign, not its magnitude Equation (6). Hence, the MK test statistic, S, is calculated from the sum of the signs of the slopes:

$$S = \sum_{i=1}^{n-1} \sum_{j=i+1}^{n} \operatorname{sgn}\left(X_j - X_i\right), \tag{5}$$

where $n =$ number of data points, $X_j =$ the j^{th} observation, and $x_i =$ the i^{th} observation where $j > i$. the sgn can be estimated as follows:

$$\operatorname{sgn}(X_j - X_i) = \begin{cases} 1 \text{ if } (X_j - X_i) > 0 \\ 0 \text{ if } (X_j - X_i) = 0 \\ -1 \text{ if } (X_j - X_i) < 0 \end{cases}. \quad (6)$$

If the null hypothesis H_0 is accepted at the significant level α, then the mean and variance of S are given by Kendall (1975), and, as it is approximately normally distributed, mean (S) is zero mean (S) = 0.

Where there are no ties in either ranking, the distribution of S may be approximated well by a normal distribution, with mean zero and variance as stated in Equation (7)):

$$\operatorname{Var}(s) = \frac{n(n-1)(2n+5)}{18}. \quad (7)$$

The normal approximation, Z statistics, is stated in Equation (8) as follows:

$$Z = \begin{cases} \dfrac{S-1}{\sqrt{\operatorname{Var}(s)}} \text{ if } S > 0 \\ 0 \text{ if } S > 0 \\ \dfrac{S+1}{\sqrt{\operatorname{Var}(s)}} \text{ if } S < 0 \end{cases}. \quad (8)$$

S values that are positive or negative represent an upward or downward trend, respectively. Subsequently, the absolute value of Z must be compared with the typical, regular accumulated distribution to ascertain whether a statistically significant trend exists at the chosen level of significance (0.05) Equation (8). The trend is increasing if Z is positive, declining if negative. The absolute value of Z must be bigger than $Z/2$ to reject the null hypothesis of no trend (H_0), where is the selected level of significance (for example, 5%), and Z 0.025 = 1.96, which can be found in conventional normal cumulative distribution tables.

3.2. SWAT Model Application and Governing Equations. The SWAT model is flexible and can incorporate a variety of environmental processes, etc., so it is used frequently. In smaller catchments where the vegetation, soil, and land utilization class are uniform, elementary hydrologic response structures are mainly square. The model requires spatial data, such as slope, soil, land use and cover maps, and DEM data, as well as temporal meteorological data, such as precipitation, temperature, relative humidity, solar radiation, and wind speed, as inputs.

3.3. SWAT Model Watershed Delineation. The Shafe watershed covers 144.47 km^2 with 11 subbasins, and was delineated using manually added outlet and automatically delineated catchment area (Table 4). Once the watershed is delineated, hydrologic response unit (HRU) analysis takes place. The input for HRU is land use, soil and slope data, and divides each subbasin into HRUs with a unique LULC, soil, and slope combination (Figure 6). The delineated watershed and soil map overlap 100%.

Table 4: Shafe soil types.

Soil type	Area (km^2)
Chromic vertisols	2.70
Dystric fluvisols	38.63
Dystric nitisols	36.79
Orthic acrisols	66.35

In HRU, the Shafe watershed was further classified into five slope categories—0%–2%, 2%–10%, 10%–15%, 15%–30%, and 30%–99%—using the SWAT interface. All three maps (land use, soil, and topography) were overlaid to create a total of 128, 153, and 152 HRUs with unique land cover/soil and slope classes for 1998, 2009, and 2021 LULC, respectively. The land use, soil, and slope datasets were imported, overlaid, and linked with the SWAT databases (Figures 6(b), 7, and 8(a)). The HRU definition options used a 5% land use, 10% soil, and 5% slope thresholds as the definition basis (Figure 8(b)). The LULC symbols (SWAT codes) are presented in Table 5.

3.4. SWAT Model Simulation and Sensitivity Analysis. In this study, SWAT model streamflow parameter sensitivity analysis was performed using SWAT CUP with the SUFI-2 algorithm. The analysis was carried out over 17 years, including a 3-year warm-up period (January 1, 1998–December 31, 2000) and a 14-year calibration period (January 1, 2001–December 31, 2014). The t-stat provides a measure of sensitivity, larger values indicating greater sensitivity, and the p-values determine the sensitivity's significance (p-values close to 0 indicating greater significance) [47].

3.5. Model Calibration and Validation. The SWAT model was calibrated by adjusting the values of the model-sensitive parameters until the simulated results matched the observed data. For this study, a 3-year LULC map (1998, 2009, and 2021) was prepared, and calibration was based on the watershed characteristics, including the evaluation of climate characteristics, and rainfall and slope effects in the catchment area. In addition to good model performances, the simulated and observed hydrograph well captured in the Shafe catchment.

3.6. Evaluation of SWAT Model Performance. To assess the quality and reliability of the SWAT predictions, statistical measures were used to evaluate its performance compared to observed and values (Equation (8)).

Coefficient of determination (R^2): measures the strength of the relationship between the observed and simulated values.

$$R^2 = \frac{\left[\sum_{i=1}^{n} \left(Q_{\text{sim}} - \overline{Q}_{\text{sim}}\right)\left(Q_{\text{obs}} - \overline{Q}_{\text{obs}}\right)\right]^2}{\sum_{i=1}^{n} \left(Q_{\text{sim}} - \overline{Q}_{\text{sim}}\right)^2 \left(Q_{\text{obs}} - \overline{Q}_{\text{obs}}\right)^2}. \quad (9)$$

The NSE is a measure of how well the simulated values fit the observed values on a 1 : 1 line. If the simulated and measured values are the same, NSE is 1 (Equation (11)). If NSE is between 0 and 1, it shows some deviations between the two.

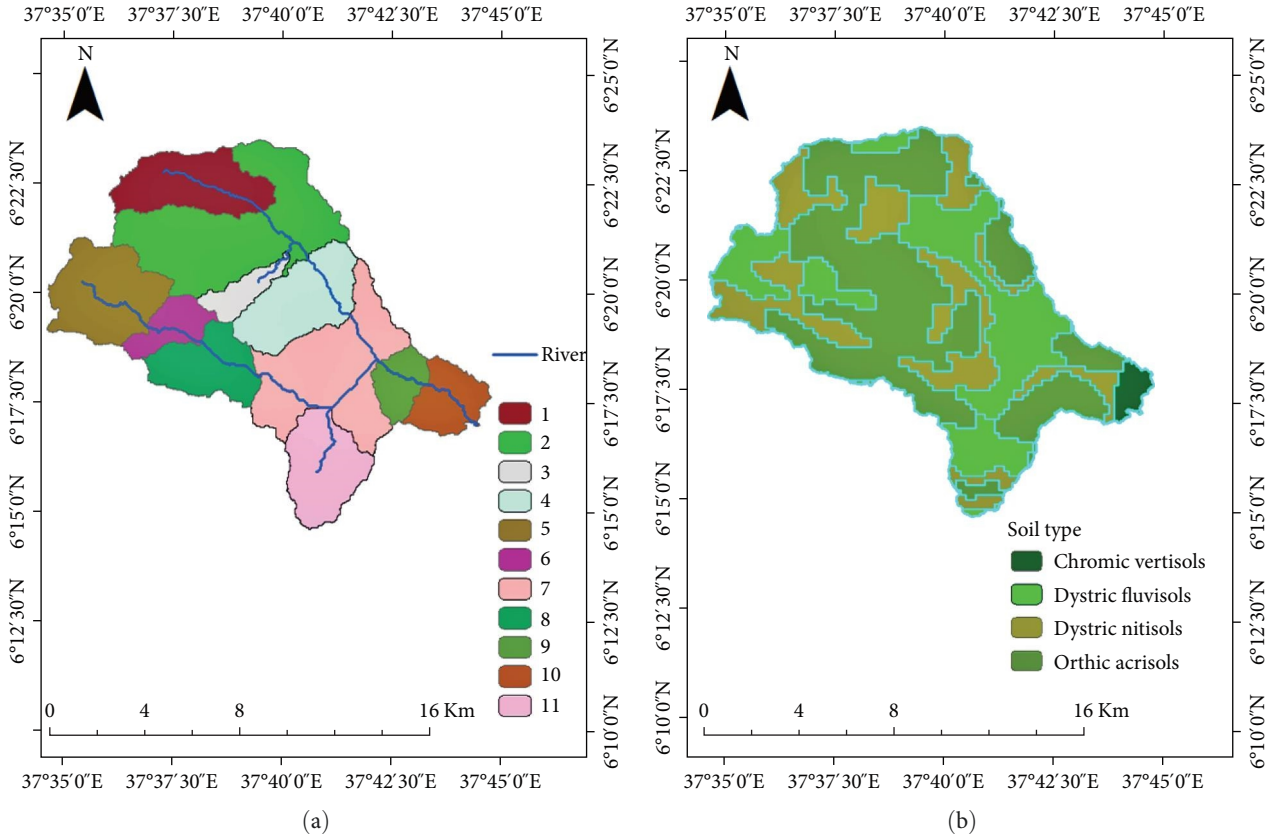

FIGURE 6: Study area and soil reclassified in the SWAT database: (a) watershed subbasins and (b) soil map.

The percent bias (PBIAS) measures the average tendency of the simulated data to be larger or smaller than the observed values. A PBIAS of zero is ideal, and low-magnitude values indicate accurate model simulation (Equation (11)).

The root-mean-square error observation standard deviation ratio (RSR) is an error index indicator. RSR ranges from 0 to 1, with values closer to zero indicating better model performance (Equation (11)). In the equations, Q_{obs} represents observed flow, as the mean of n observed values, and Q_{sim} simulated flow, as the mean of n simulated values.

According to Moriasi et al. [48], each model statistical indicator should be checked after each simulation, and calibrated to at least the minimum recommended values of $R^2 > 0.6$, NSE > 0.5, PBIAS < +20, and RSR < 0.7.

$$\mathrm{NSE} = 1 - \frac{\sum_{i=1}^{n}((Q_{obs} - Q_{sim})^2)}{\sum_{i=1}^{n}\left((Q_{obs} - \overline{Q}_{obs})^2\right)} \quad (10)$$

$$\mathrm{PBIAS} = \left[\frac{\sum_{i=1}^{n} Q_{sim} - \sum_{i=1}^{n} Q_{obs}}{\sum_{i=1}^{n} Q_{Obs}}\right] \times 100 \quad (11)$$

$$\mathrm{RSR} = \frac{\mathrm{RMSE}}{\mathrm{STDEV}_{ob}} = \frac{\sqrt{\sum_{i=1}^{n}(Q_{obs} - Q_{sim})^2}}{\sqrt{\sum_{i=1}^{n}\left(Q_{obs} - \overline{Q}_{sim}\right)^2}} \quad (12)$$

4. Results and Discussion

To evaluate how watershed factors affect streamflow, three sets of LULC and soil maps (Figure 7(b)), rainfall, and temperature data were used. LULC satellite images were analyzed in monthly time steps in the SWAT model (Figure 7). Whenever the model ran, the variables were checked, and the simulation results used to determine how the LULC change affected the hydrologic processes and streamflow. Ultimately, the streamflow that the model had simulated was assessed.

5. Historic LULC

5.1. LULC Maps (1998, 2009, and 2021). According to the 1998 LULC map, the area's dominant LULC is shrub land (38%), forest (22%), and agricultural land (21%)—the proportional areas have been rounded to the nearest whole number percent. The remaining areas are covered by grassland (19%) (Figure 7(a)). The LULC map for 2009 shows that the LULC pattern had changed: agriculture (28%), grassland (25%), shrub land (30%), and forest (18%). There was, thus, a 4% decline in forest coverage between 1998 and 2009, and a small rise in agricultural regions (Figure 7(b)). The map for 2021 showed further changes: agriculture (35%), shrub land (29%), grassland (22%), and forest (14%). In general,

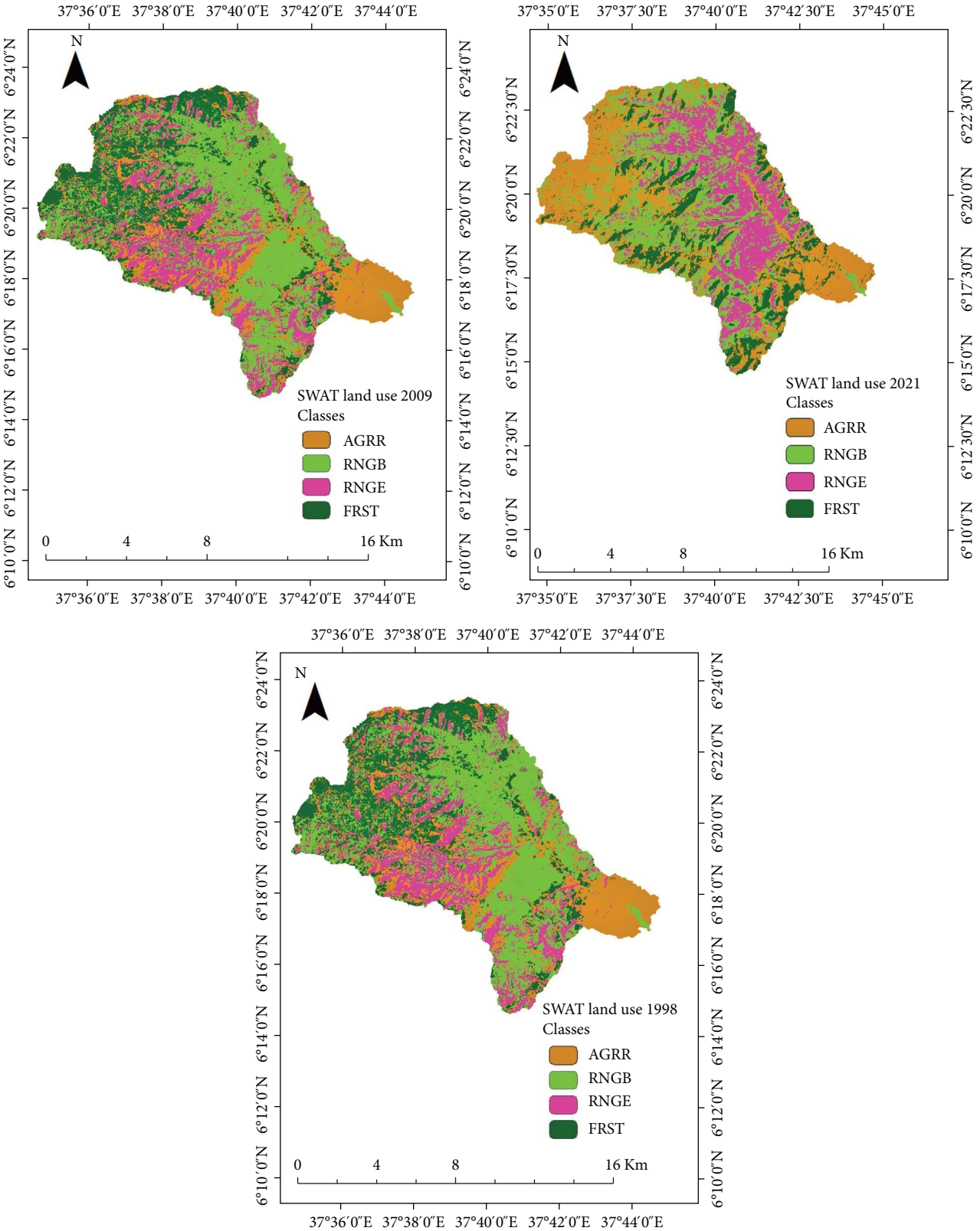

Figure 7: Land use reclassified in SWAT model 2009, 2021, and 1998.

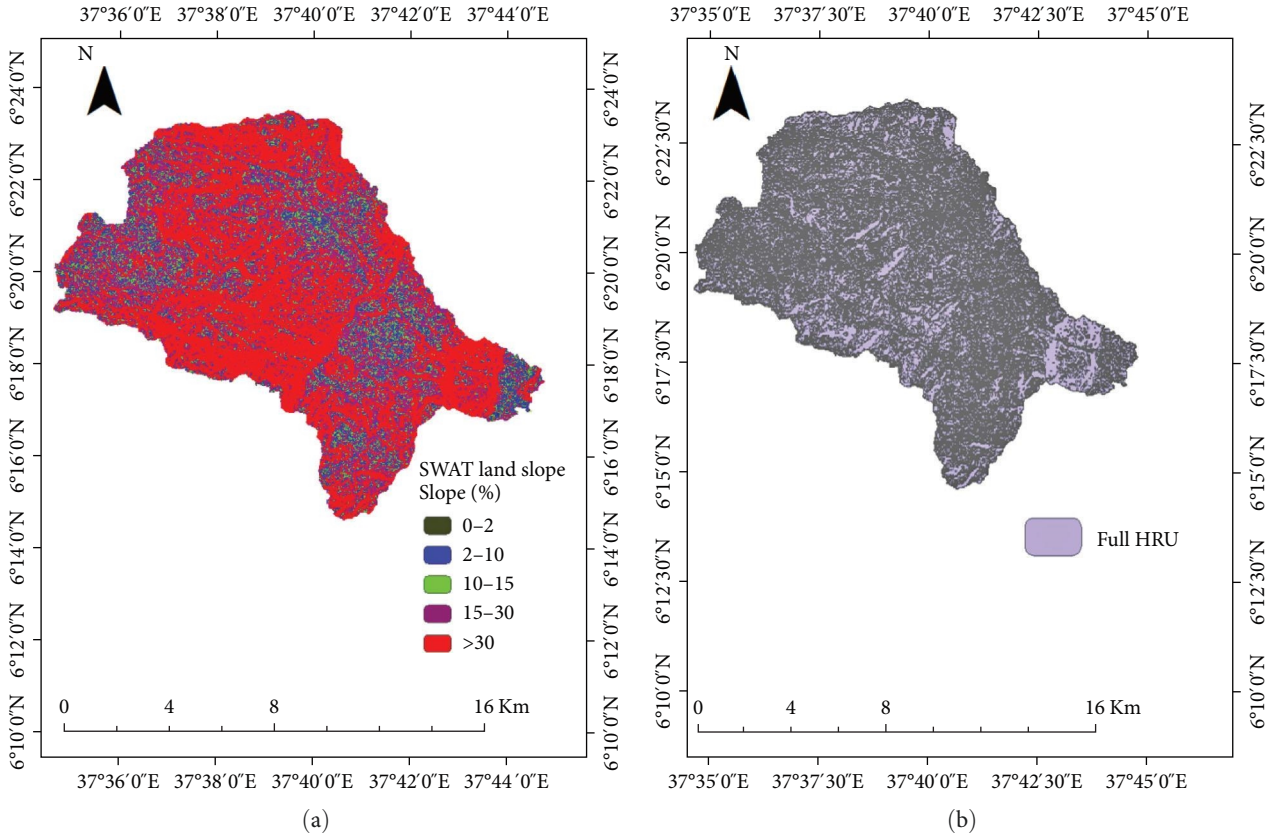

Figure 8: Reclassified slopes and full HRUs map of the Shafe catchment: (a) area slope and (b) HRU.

Table 5: LULC classifications.

LULC type	SWAT code
Agricultural land	AGRL
Forest	FRST
Shrubland	RNGB
Grassland	RNGE

therefore, the area of agricultural land increased between 1998 and 2021, while the forest area decreased (Figure 7(c)).

5.2. Identification of Autocorrelation. Prior to implementing trend tests, the autocorrelation of the RF, Q_{obs}, PET, and T_{mean} data were examined for the research period—Lag-1 autocorrelation coefficient value were calculated for all seasonal series and all stations. Calculating Lag-1 for each hydroclimatic variable and season, including annual time-series data, enabled the significance of Lag-1 autocorrelation to be evaluated. As a result, autocorrelation was shown for the winter season time-series for all hydroclimatic variables in the watershed for the period 1998 to 2021. The summer season time-series data were not autocorrelated, however. For the spring season time-series only Q_{obs} and PET were found to have autocorrelations. The annual Q_{obs}, T_{mean}, and PET series, as well as the autumn season RF, Q_{obs}, and PET series, were shown to be autocorrelated at the catchment's station (Figure 9(a)–9(h). The series' remaining seasons and the full set of stations were unrelated.

Table 6 is a full comparison of z_{sb} and z_{sa}, and shows that z_{sa} is lower than z_{sb} in all seasons, indicating a more negative trend in the RF and Q_{obs} time series between 1998–2021. This suggests that z_{sa} is a more sensitive indicator of the trend in the variable than z_{sb}. Comparing p-value with $\dot{p}$, it can be seen that $\dot{p}$ is lower than p-value for all seasons, suggesting that $\dot{p}$ is a more significant indicator of the trend in the variable's statistical significance than p-value.

Winter, spring, summer, autumn, and annual hydro climatic variable mean seasonal and annual trends are shown in Table 7 for the research area. The MK analysis in R-package and R-studio was used to look at regional patterns and hydro climatic variability in the watershed. The mean seasonal temperature trends showed statistically significant increases on average in all seasons except winter, at a 95% level of significance. There were statistically significant downward seasonal trends on average, however, in all seasons except spring.

In the watersheds, the mean seasonal streamflow revealed declining trends that were statistically significant in winter and spring, but nonsignificant at the 5% level of confidence in summer and autumn (p-value 0.05). The seasonal PET patterns show that there were upward tendencies throughout the year. With the exception of the spring PET trend, there is a strong upward tendency in every season (Table 7). The average annual temperature is increasing but not significantly. While the mean annual PET was significantly rising during

Figure 9: Seasonal and annual autocorrelation coefficient at Lag-1 catchment's station.

Table 6: Trends before and after autocorrelation.

Stations	z_{sb}	z_{sa}	p-Value	$\dot{p}$	S1	S2
T_{mean}						
Winter	2.03	1.63	0.00	0.10	21.4	1.30
Annual	1.86	1.44	0.08	0.07	13.1	4.10
RF						
Winter	−1.41	−2.82	0.08	0.02	4.6	−2.54
Autumn	−2.16	−2.52	0.01	0.00	3.6	−1.85
PET						
Winter	3.96	2.39	0.09	0.00	2.4	−2.57
Spring	3.22	1.60	0.22	0.11	8.7	−1.12
Autumn	3.56	2.6	0.60	0.00	1.81	−1.85
Annual	2.52	2.27	0.03	0.00	1.57	−6.70
Q_{obs}						
Winter	−1.647	−2.67	0.08	0.02	1.17	−15.45
Spring	−2.02	−2.8	0.04	0.00	2.1	−12.71
Annual	3.284	−1.97	0.15	0.01	2.8	1.27

Table 7: Mean seasonal trends of climatic variable in the watershed.

Season	Z	p Value	S	Sig.	Season	Z	p Value	S	Sig.
		T_{mean}					RF		
Winter	1.63	0.10	0.01	–	Winter	−2.82	0.02	−2.54	**
Spring	2.53	0.01	0.01	**	Spring	−0.92	0.36	−1.55	–
Summer	2.52	0.01	0.01	**	Summer	−3.52	0.00	−1.85	**
Autumn	2.07	0.00	0.01	**	Autumn	−2.52	0.01	−1.21	**
		PET					Observed flow		
Winter	2.39	0.00	0.48	**	Winter	−2.67	0.01	15.45	**
Spring	1.60	0.11	−1.12	–	Spring	−2.02	0.04	12.711	**
Summer	2.22	0.00	−1.23	**	Summer	1.43	0.15	3.01	–
Autumn	2.27	0.00	−1.85	**	Autumn	1.06	0.29	11.00	–

Table 8: Mean annual climatic variable trends.

	Z	p Value	S	Sig.		Z	p Value	S	Sig.
		T_{mean}					Rainfall		
Annual	1.44	0.15	0.01	–	Annual	−2.42	0.02	−8.04	**
		PET					Observed flow		
Annual	−1.98	0.00	−6.70	**	Annual	2.38	0.01	1.27	**

the trends analysis (Table 8), the streamflow and rainfall showed significantly declining trends. A statistical analysis of the trends' significance is also provided in the table, with the symbol, **, designating trends that are statistically significant at levels of 0.05.

5.3. Hydrologic Model Sensitivity, Calibration, and Validation

5.3.1. Sensitivity Analysis. The SWAT hydrologic model sensitivity analysis was done using SUFI-2 and identified the most sensitive model parameters in the watershed over the warmup, calibration, and validation periods. Three of the 19 variables evaluated—CN2, ALPHA_BF, and CH-K2—displayed substantial sensitivity, the other five showed low sensitivity. As demonstrated in Table 9 and Figure 10, just four-variables exhibited a small degree of sensitivity, and the remaining variables had little or no influence on the result [49, 50].

5.3.2. SWAT Calibration and Validation. SWAT's performance was evaluated using default SWAT CUP parameters before calibration. The simulated flow captured the observed hydrograph poorly. Figures 11–13 are the catchment's simulated and observed monthly hydrographs for the calibration and validation periods. The model captured the hydrograph

Table 9: Shafe watershed sensitive model parameters and ranks.

Parameter name	Description	*t*-Stat	*p*-Value	Rank	Sensitivity
ALPHA_BF	Alpha base flow recession constant	−107.30	0.001	1	High
CN2	SCS runoff curve number	−17.29	0.009	2	High
CH_K2	Effective hydraulic conductivity in main channel	10.96	0.010	3	High
ESCO	soil evaporation compensation factor	−1.62	0.106	4	Moderate
EPCO	Plant uptake compensation factor	−1.56	0.119	5	Moderate
SOL_AWC	Available water content of soil	−1.13	0.259	6	Moderate
SLSUBBSN	Average slope length	1.10	0.272	7	Moderate
SOL_Z	Soil depth (for each layer)	0.87	0.387	8	Moderate
SURLAG	Surface runoff lag time	−0.73	0.468	9	Low
GWQMN	Threshold depth of water in the shallow aquifer	−0.66	0.511	10	Low
RCHRG_DP	Deep aquifer percolation fraction	−0.56	0.574	11	Low
GW_REVAP	Groundwater "revap" coefficient	−0.56	0.577	12	Low
REVAPMN	Threshold depth of water in the aquifer for "revap" to occur	−0.53	0.596	13	Least
CH_S2	Average slope of main channel	0.49	0.627	14	Least
CANMX	Maximum canopy storage	−0.37	0.712	15	Least
SOL_K	Saturated hydraulic conductivity	0.35	0.725	16	Least
PPERCO	Phosphorus percolation coefficient	0.35	0.726	17	Least
CH_N2	Manning's *n*" value for the main channel	−0.31	0.759	18	Least
GW_DELAY	Groundwater delay	0.20	0.842	19	Least

recession limb and base flow well, but underestimated some peak flows. The general pattern of the observed hydrograph was not captured perfectly due to poor quality and sparsely distributed rain gauges, which might cause rating curve problems, and a combination of the significant increase in agricultural activity, and deterioration of the catchment's forestland, trees, and shrubs. Figure 13 depicts the maximum streamflow rate for the LULC reported for 2021. The modeled streamflows were, however, only moderate for the LULCs of both 1998 and 2009 (Figures 11 and 12).

The SUFI-2 uncertainty measure for each LULC was determined. For LULC 1998, the *p*-factor of 0.78 and *r*-factor of 0.92, for LULC 2009, the *p*-factor of 0.70 and *r*-factor of 0.88, and for LULC 2021, the *p*-factor of 0.70 and *r*-factor of 0.77 were obtained. This showed that, the 95 PPU band incorporated about 78% of the 1998 LULC data, and 70% of the 2009 and 2021 LULC data, with a better strength of estimation (*r*-factor < 1) for all cases (Table 10).

Table 11 shows the catchment's SWAT object functions in the three LULC scenarios. During calibration, the NSE exceeded 0.6 for each LULC period. This suggested that the very good performances of model simulated flow in capturing the observed hydrograph pattern. For the 1998 LULC, the PBIAS values were within ± 5 5%, indicating that the model reproduced observed streamflow volumes well. The model assessment of performance requirements for stream calibration and verification for the three LULCs demonstrated good performance with R^2 greater than 0.72, NSE greater than 0.66, and RSR within the permissible range.

5.3.3. Hydrologic Process Responses to LULC Change. LULC change has significant impact on watershed hydrologic processes including runoff, groundwater flow, infiltration, erosion, and evapotranspiration. Monthly simulation runs were conducted using the 1998, 2009, and 2021 LULC maps. A comparison of model-simulated streamflow for 1998, 2009, and 2021 and average annual observed streamflow from the watershed showed significant changes, and the results were presented in a table. The findings indicated a 16% increase in 2009′s median annual stream discharge compared to that of 1998. Additionally, LULC 2021 simulated mean annual streamflow increased by 13.03% from 2009 LULC (Table 12). The increases in agricultural land between 1998, 2009, and 2021, reduced infiltration and increased runoff. Streamflow decreased when afforestation increased.

The features of different kinds of land cover have been demonstrated to be directly related to the watershed's yearly mean streamflow. While the frost area dropped every eleven years between 1998 and 2021, the amount of cultivated and agricultural land expanded in the study area, during the study period. By lowering infiltration in the watersheds, the extension of agricultural land increased streamflow (Figure 14). However, as observed by Sun et al. [51] shrub and woodland have the potential to reduce streamflow due to decreased infiltration.

5.4. Meteorological Data Effect on Streamflow

5.4.1. PET Effect on Streamflow. The length of a meteorological dataset can affect runoff through evapotranspiration and rainfall in the catchment. The humidity index (HI) is used in

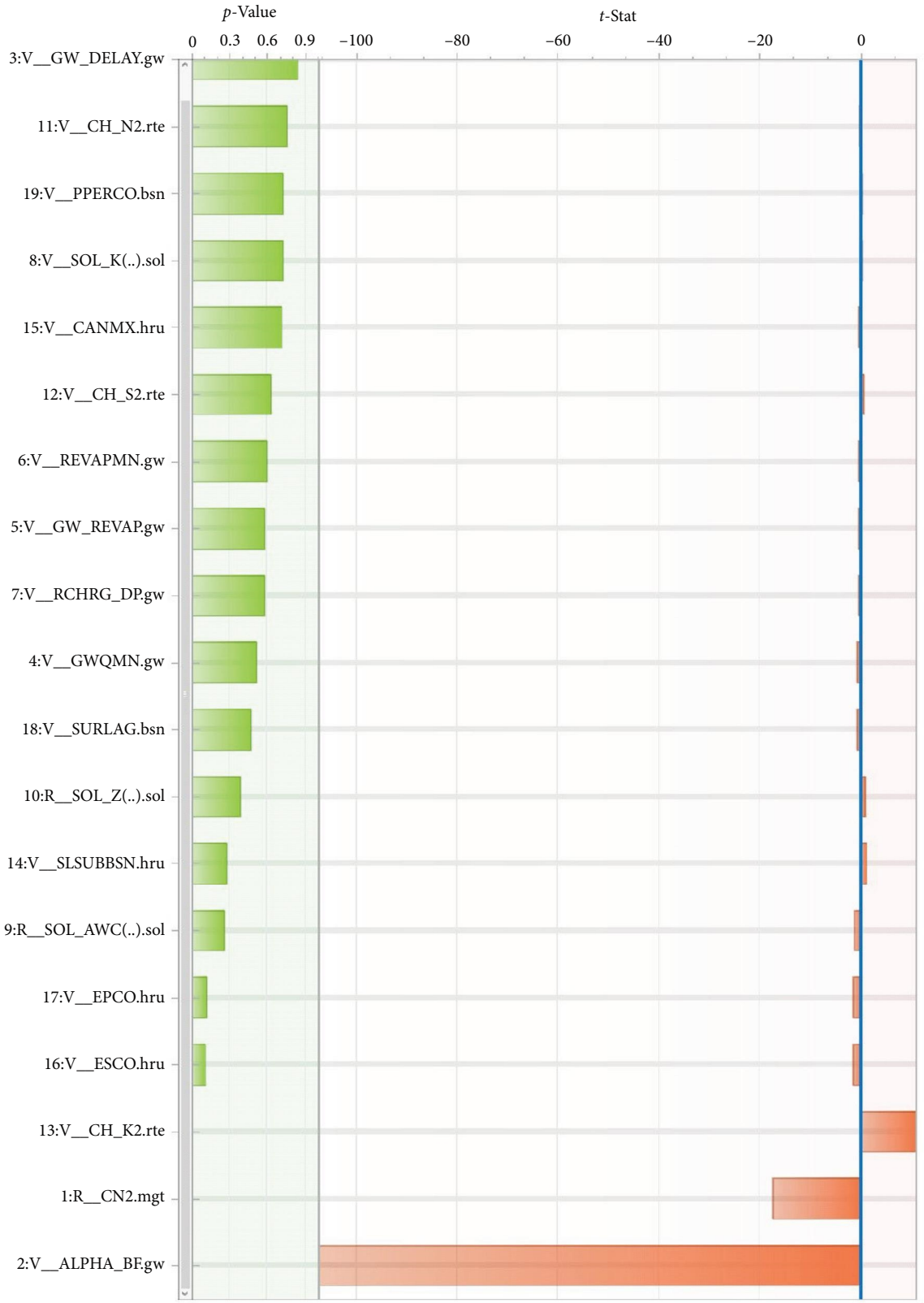

Figure 10: Sensitive flow parameters depending on p-value and t-test.

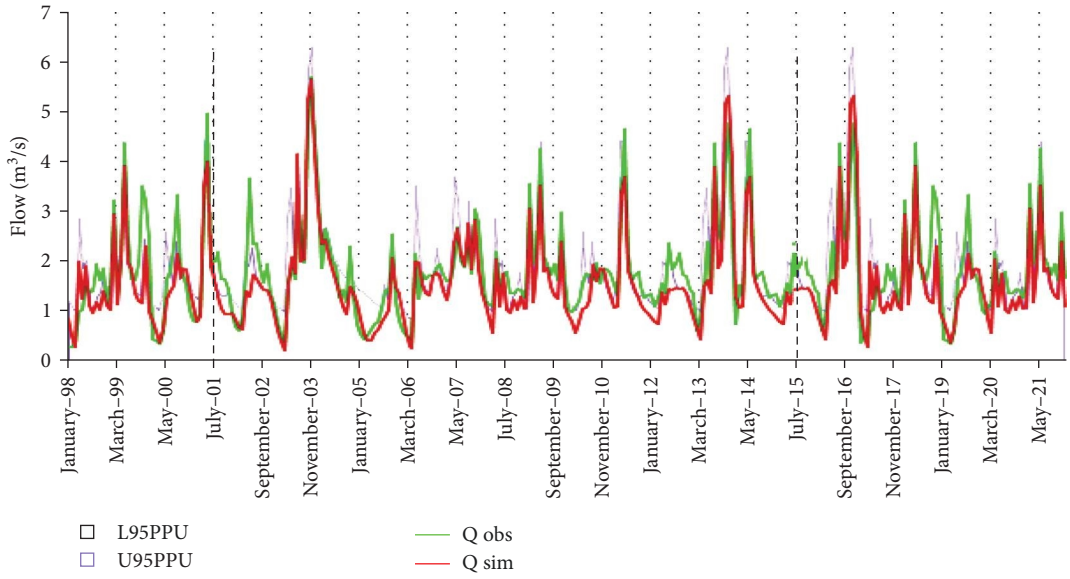

Figure 11: Observed and simulated hydrograph for LULC 1998.

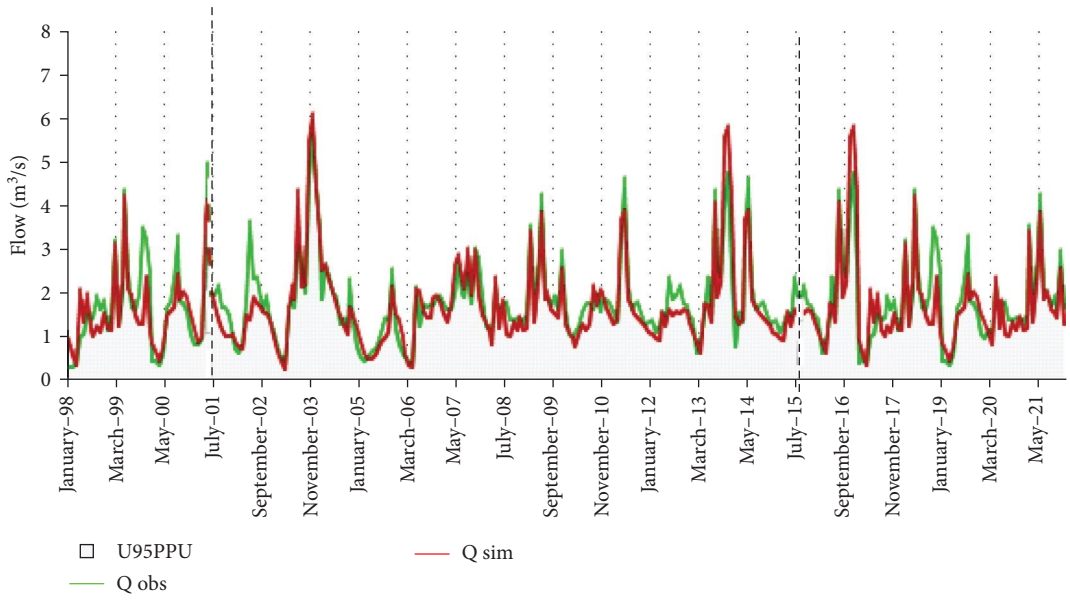

Figure 12: Observed and simulated hydrograph for LULC 2009.

this study to represent the mean annual rainfall divided to mean annual evapotranspiration. It indicates how much atmospheric moisture demand is satisfied by precipitation. The climate index is an essential parameter to analyze the effect of climate on streamflow by comparing the climate index value. The higher the climate index, the more streamflow discharge is generated by the watershed, while lower values show that the watershed generates little discharge. In this study, the climate index effect on streamflow was evaluated using a 12-year climate data interval.

In Case 1, using station data from 1998 to 2011, the long-term 12-year average annual rainfall was 1,095 mm, and the potential evapotranspiration, from the SWAT model, was 1,227 mm. The climate index was calculated by dividing the average annual rainfall by the evapotranspiration, giving 0.89. The annual streamflow was estimated as 39.03 mm/year. In Case 2, using climate data from 2012 to 2021 the long-term annual rainfall was 1061.0 mm/year, and the annual evapotranspiration from the SWAT model was 1,143.8 mm/year. The climate index was calculated as above and was 0.93. The simulated annual streamflow from the SWAT model was recorded at 40.81 mm/year. According to Seong et al. [52]), a higher humidity index indicates a wetter watershed than a lower one. The model output showed that when the humidity index was higher, the annual watershed streamflow was 40.81 mm, but streamflow was reduced to 39.03 mm at the lower HI. From the first 13 years of meteorological data to the second 13 years of meteorological data, the average yearly

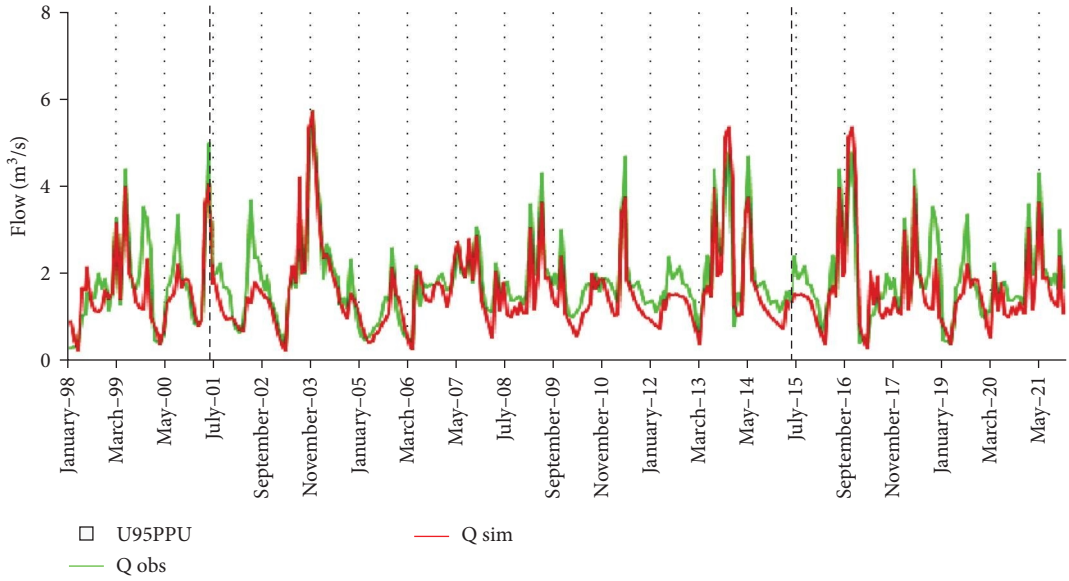

Figure 13: Observed and simulated hydrograph for LULC 2021.

Table 10: Suggested and calibrated flow parameters.

Parameter name	Effects of parameters in runoff when it increases	Manual range	Calibration range	Fitted value
CN2	Increase surface runoff	35–98	±25%	0.36
ALPHA_BF	Increase groundwater flow	0–1	0.01–0.135	0.06
GWQMN	Decrease baseflow	0–5,000	3,000–4,000	3,837.00
GW_REVAP	Decrease baseflow by increasing water transfer in shallow aquifer	0.02–0.2	0.1–0.15	0.14
RCHRG_DP	Decrease baseflow by deep aquifer	0–1	0.95–1	0.99
SOL_AWC	Increase groundwater recharge	0–1	0.96–1	0.98
SOL_Z	Increase groundwater	0–3,500	±25%	0.99
CH_K2	Saturated hydraulic conductivity	0–500	98–108	106.22
SLSUBBSN	increase surface runoff	10–150	25–30	28.16
ESCO	Decrease evaporation	0–1	0.96–1	0.97
EPCO	Decrease transpiration	0–1	0.0–0.1	0.07
SURLAG	Decrease runoff arrival time to outlet	0.05–24	14–15	14.37

Table 11: SWAT performance in the calibration and validation periods.

		Calibration (2001–2014) model performance				Validation (2015–2021) model performance			
p-Factor	*r*-Factor	R^2	NSE	PBIAS	RSR	R^2	NSE	PBIAS	RSR
LULC 1998									
0.78	0.92	0.76	0.74	4.4	0.52	0.72	0.72	7.0	0.53
LULC 2009									
0.70	0.88	0.76	0.72	11.0	0.53	0.85	0.66	16.7	0.58
LULC 2021									
0.70	0.77	0.76	0.73	10.9	0.52	0.84	0.66	16.4	0.58

Table 12: Simulated mean annual streamflow.

	LULC 1998	LULC 2009	LULC 2021
Simulated streamflow (mm)	39.40	46.93	53.92

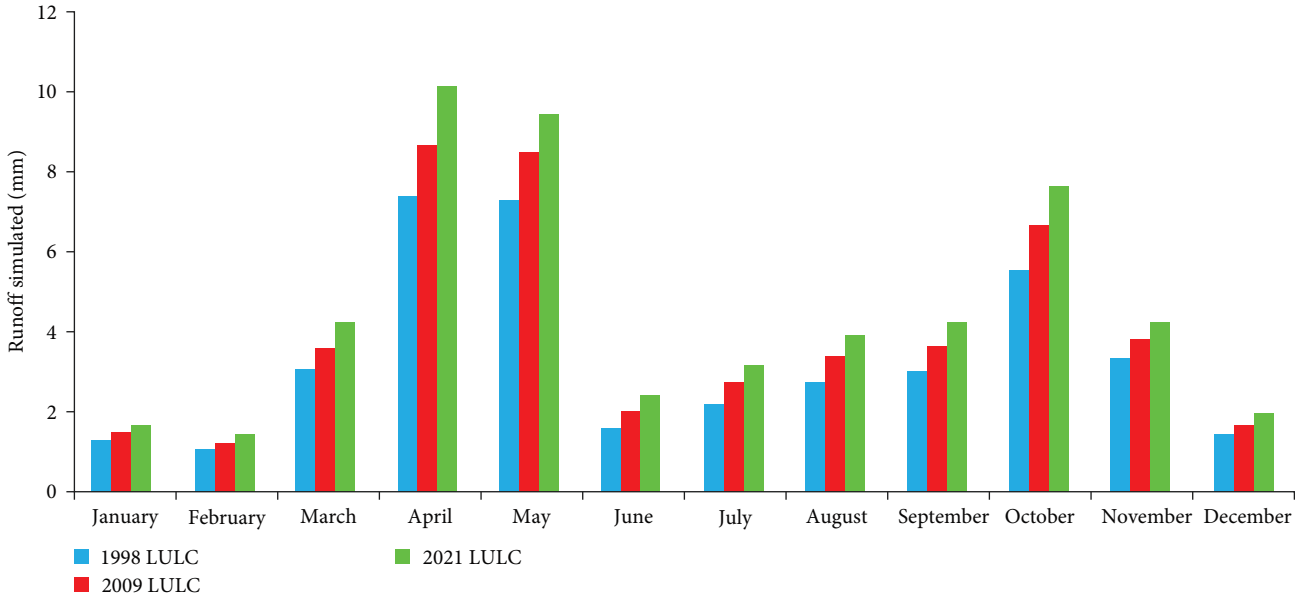

Figure 14: Simulated monthly streamflow (by LULC).

flow of streams of the watershed declined by 2.87%. This indicates that meteorological data in and around the catchment can affect stream flow.

5.4.2. Rainfall Effects on Streamflow. By only changing the rainfall data intervals, the effect on streamflow was evaluated. The model output for the first 13 years (1998–2011) was 37.21 mm/year, and for the next 13 years (2012–2021), it was 35.86 mm/year. The mean annual precipitation fell between 1,095.6 and 1,061.0 mm throughout the course of the first 13 years to the second 13 years, a 3.2% loss. The yearly streamflow also fell by 3.76% in addition. These results imply that rainfall intensity has a substantial impact on streamflow in the Shafe catchment.

6. Conclusions

This study assessed the Shafe catchment in the rift valley lakes basin physical and climate catchment characteristics effect on stream. The SWAT model was used to investigate the influence of watershed variables. The model successfully reproduced the reported hydrograph patterns and volumes under various LULC conditions. Twelve model parameters were found for calibration by sensitivity analysis, which led to excellent model performance with high R^2 and NSE values, and low PBIAS and RSR. According to the study, changes in LULC, particularly the increases in agricultural land and deforestation, had a major impact on monthly flow in the watershed. The study suggested that the optimum land use management techniques for reducing streamflow were to decrease agricultural land and increase afforestation. Watershed influences on streamflow should be taken into account in water resource planning and management. For a variety of water resource studies, including water budget studies, physical catchment features can be employed as an alternative data source. To lessen the detrimental effect on streamflow, LULC changes should be monitored and controlled efficiently.

Data Availability

The data used are confidential and not publicly available due to data protection reasons.

Conflicts of Interest

The authors declare that they have no known competing financial interests or personal relationships that could have appeared to influence the work reported in this paper.

Authors' Contributions

This research was conceptualized and designed by Zerihun Makayno Mada and Abera Shigute Nannawo. Zerihun Makayno Mada conducted the samples/material collection and preparation. Both Zerihun Makayno Mada and Abera Shigute Nannawo analyzed samples, collected data, and did statistical analysis. Zerihun Makayno Mada wrote the first draft of the manuscript, and both authors read and commented on previous versions of the manuscript and approved the final manuscript for submission.

References

[1] S. E. Chaemiso, S. A. Kartha, and S. M. Pingale, "Effect of land use/land cover changes on surface water availability in the Omo-Gibe basin, Ethiopia," *Hydrological Sciences Journal*, vol. 66, no. 13, pp. 1936–1962, 2021.

[2] A. S. Nannawo, T. K. Lohani, and A. A. Eshete, "Envisaging the actual evapotranspiration and elucidating its effects under climate change scenarios on agrarian lands of bilate river basin in Ethiopia," *Heliyon*, vol. 8, no. 8, Article ID e10368, 2022.

[3] R. K. Adhikari, S. Mohanasundaram, and S. Shrestha, "Impacts of land-use changes on the groundwater recharge in the Ho Chi Minh city, Vietnam," *Environmental Research*, vol. 185, Article ID 109440, 2020.

[4] A. Chemura, D. Rwasoka, O. Mutanga, T. Dube, and T. Mushore, "The impact of land-use/land cover changes on water balance of the heterogeneous Buzi sub-catchment, Zimbabwe," *Remote Sensing Applications: Society and Environment*, vol. 18, Article ID 100292, 2020.

[5] L. Nkhoma, C. Ngongondo, Z. Dulanya, and M. Monjerezi, "Evaluation of integrated impacts of climate and land use change on the river flow regime in Wamkurumadzi river, shire basin in Malawi," *Journal of Water and Climate Change*, vol. 12, no. 5, pp. 1674–1693, 2021.

[6] C. C. Nnaji, N. M. Ogarekpe, and E. J. Nwankwo, "Temporal and spatial dynamics of land use and land cover changes in derived savannah hydrological basin of Enugu State, Nigeria," *Environment, Development and Sustainability*, vol. 24, pp. 9598–9622, 2022.

[7] S. Y. Birhanu, M. A. Moges, B. G. Sinshaw et al., "Hydrological modeling, impact of land-use and land-cover change on hydrological process and sediment yield; case study in Jedeb and Chemoga watersheds," *Energy Nexus*, vol. 5, Article ID 100051, 2022.

[8] A. Sood, L. Muthuwatta, N. S. Silva, and M. McCartney, *Understanding the Hydrological Impacts of Climate Change in the Tana River Basin, Kenya*, International Water Management Institute (IWMI), Colombo, Sri Lanka, 2017.

[9] A. S. Nannawo, T. K. Lohani, and A. A. Eshete, "Exemplifying the effects using WetSpass model depicting the landscape modifications on long-term surface and subsurface hydrological water balance in Bilate basin of Ethiopia," *Advances in Civil Engineering*, vol. 2021, Article ID 7283002, 20 pages, 2021.

[10] M. Belihu, S. Tekleab, B. Abate, and W. Bewket, "Hydrologic response to land use land cover change in the upper Gidabo watershed, rift valley lakes basin, Ethiopia," *HydroResearch*, vol. 3, pp. 85–94, 2020.

[11] E. Mutayoba, J. J. Kashaigili, F. C. Kahimba, W. Mbungu, and N. A. Chilagane, "Assessing the impacts of land use and land cover changes on hydrology of the mbarali river sub-catchment. The case of upper great ruaha sub-basin, Tanzania," *Engineering*, vol. 10, no. 9, pp. 616–635, 2018.

[12] E. Assefa and H.-R. Bork, "Dynamics and driving forces of agricultural landscapes in southern Ethiopia—a case study of the Chencha and Arbaminch areas," *Journal of Land Use Science*, vol. 11, no. 3, pp. 278–293, 2016.

[13] A. S. Nannawo, T. K. Lohani, A. A. Eshete, and M. T. Ayana, "Evaluating the dynamics of hydroclimate and streamflow for data-scarce areas using MIKE11-NAM model in Bilate river basin, Ethiopia," *Modeling Earth Systems and Environment*, vol. 8, pp. 4563–4578, 2022.

[14] A. S. Nannawo, T. K. Lohani, and A. A. Eshete, "Groundwater recharge evaluation due to climate change using WetSpass-M distributed hydrological model in Bilate river basin of Ethiopia," *Groundwater for Sustainable Development*, vol. 19, Article ID 100860, 2022.

[15] A. G. Nigusse and O. G. Adhanom, "Flood hazard and flood risk vulnerability mapping using geo-spatial and MCDA around Adigrat, Tigray region, northern Ethiopia," *Momona Ethiopian Journal of Science*, vol. 11, no. 1, 2019.

[16] M. R. Aredo, S. D. Hatiye, and S. M. Pingale, "Impact of land use/land cover change on stream flow in the Shaya catchment of Ethiopia using the MIKE SHE model," *Arabian Journal of Geosciences*, vol. 14, Article ID 114, 2021.

[17] V. Balthazar, V. Vanacker, A. Molina, and E. F. Lambin, "Impacts of forest cover change on ecosystem services in high Andean mountains," *Ecological Indicators*, vol. 48, pp. 63–75, 2015.

[18] R. DeFries and K. N. Eshleman, "Land-use change and hydrologic processes: a major focus for the future," *Hydrological Processes*, vol. 18, no. 11, pp. 2183–2186, 2004.

[19] V. Roth, T. Lemann, G. Zeleke, A. T. Subhatu, T. K. Nigussie, and H. Hurni, "Effects of climate change on water resources in the upper Blue Nile Basin of Ethiopia," *Heliyon*, vol. 4, no. 9, Article ID e00771, 2018.

[20] M. G. Genjebo, A. Kemal, and A. S. Nannawo, "Assessment of surface water resource and allocation optimization for diverse demands in Ethiopia's upper Bilate Watershed," *Heliyon*, vol. 9, no. 10, Article ID e20298, 2023.

[21] H. Shiferaw, A. Gebremedhin, T. Gebretsadkan, and A. Zenebe, "Modelling hydrological response under climate change scenarios using SWAT model: the case of Ilala watershed, northern Ethiopia," *Modeling Earth Systems and Environment*, vol. 4, pp. 437–449, 2018.

[22] H. Wu, J. Zhang, Z. Bao et al., "Runoff modeling in ungauged catchments using machine learning algorithm-based model parameters regionalization methodology," *Engineering*, 2022.

[23] A. T. Tsegaw, M. Pontoppidan, E. Kristvik, K. Alfredsen, and T. M. Muthanna, "Hydrological impacts of climate change on small ungauged catchments—results from a global climate model–regional climate model–hydrologic model chain," *Natural Hazards and Earth System Sciences*, vol. 20, no. 8, pp. 2133–2155, 2020.

[24] A. Viglione, J. Parajka, M. Rogger et al., "Comparative assessment of predictions in ungauged basins—Part 3: runoff signatures in Austria," *Hydrology and Earth System Sciences*, vol. 17, no. 6, pp. 2263–2279, 2013.

[25] M. Hrachowitz, H. H. G. Savenije, G. Blöschl et al., "A decade of predictions in ungauged basins (PUB)—a review," *Hydrological Sciences Journal*, vol. 58, no. 6, pp. 1198–1255, 2013.

[26] J. Samuel, P. Coulibaly, M. Asce, and R. A. Metcalfe, "Estimation of continuous streamflow in ontario ungauged basins: comparison of regionalization methods," *Journal of Hydrologic Engineering*, vol. 16, no. 5, pp. 447–459, 2011.

[27] O. P. Abimbola, J. Wenninger, R. Venneker, and A. R. Mittelstet, "The assessment of water resources in ungauged catchments in Rwanda," *Journal of Hydrology: Regional Studies*, vol. 13, pp. 274–289, 2017.

[28] M. Sivapalan, K. Takeuchi, S. W. Franks et al., "IAHS decade on predictions in ungauged basins (PUB), 2003–2012: shaping an exciting future for the hydrological sciences," *Hydrological Sciences Journal*, vol. 48, no. 6, pp. 857–880, 2003.

[29] J. B. Swain and K. C. Patra, "Streamflow estimation in ungauged catchments using regionalization techniques," *Journal of Hydrology*, vol. 554, no. August, pp. 420–433, 2017.

[30] C. Tamalew and A. Kemal, "Estimation of discharge for ungauged catchments using rainfall–runoff model in Didessa sub-basin: the case of blue Nile river basin, Ethiopia,"

International Journal of Innovations in Engineering Research and Technology, vol. 3, no. 9, pp. 1–11, 2016.

[31] Y. Zhang and F. H. S. Chiew, "Relative merits of different methods for runoff predictions in ungauged catchments," *Water Resources Research*, vol. 45, no. 7, 2009.

[32] O. Laassilia, D. Ouazar, A. Bouziane, and M. D. Hasnaoui, "Estimation of excess water in the Sebou basin for an interbasin water transfer," *Journal of Applied Water Engineering and Research*, vol. 9, no. 1, pp. 69–87, 2021.

[33] L. Purvis and A. Dinar, "Are intra- and inter-basin water transfers a sustainable policy intervention for addressing water scarcity?" *Water Security*, vol. 9, Article ID 100058, 2020.

[34] T. H. M. Rientjes, B. U. J. Perera, A. T. Haile, P. Reggiani, and L. P. Muthuwatta, "Regionalisation for lake level simulation—the case of lake Tana in the upper blue Nile, Ethiopia," *Hydrology and Earth System Sciences*, vol. 15, no. 4, pp. 1167–1183, 2011.

[35] L. Oudin, V. Andréassian, C. Perrin, C. Michel, and N. Le Moine, "Spatial proximity, physical similarity, regression and ungaged catchments: a comparison of regionalization approaches based on 913 French catchments," *Water Resources Research*, vol. 44, no. 3, 2008.

[36] R. Merz and G. Blöschl, "Regionalisation of catchment model parameters," *Journal of Hydrology*, vol. 287, no. 1–4, pp. 95–123, 2004.

[37] G. Bloschl and M. Sivapalan, "Scale issues in hydrological modelling: a review," *Hydrological Processes*, vol. 9, no. 3-4, pp. 251–290, 1995.

[38] S. Patel, M. K. Hardaha, M. K. Seetpal, and K. K. Madankar, *Multiple linear regression model for stream flow estimation of Wainganga river*, vol. 2, no. 1, 2016.

[39] S. T. Owolabi, K. Madi, and A. M. Kalumba, "Comparative evaluation of spatio–temporal attributes of precipitation and streamflow in buffalo and tyume catchments, eastern cape, South Africa," *Environment, Development and Sustainability*, vol. 23, pp. 4236–4251, 2021.

[40] A. Belay, T. Demissie, J. W. Recha et al., "Analysis of climate variability and trends in southern Ethiopia," *Climate*, vol. 9, no. 6, Article ID 96, 2021.

[41] T. Worku, D. Khare, and S. K. Tripathi, "Spatiotemporal trend analysis of rainfall and temperature, and its implications for crop production," *Journal of Water and Climate Change*, vol. 10, no. 4, pp. 799–817, 2019.

[42] R. Rustum, A. J. Adeloye, and F. Mwale, "Spatial and temporal trend analysis of long term rainfall records in data-poor catchments with missing data, a case study of lower shire floodplain in malawi for the period 1953–2010," *Hydrology and Earth System Sciences*, 2017.

[43] A. E. Harka, N. B. Jilo, and F. Behulu, "Spatial–temporal rainfall trend and variability assessment in the upper wabe shebelle river basin, Ethiopia: application of innovative trend analysis method," *Journal of Hydrology: Regional Studies*, vol. 37, Article ID 100915, 2021.

[44] G. Bayable, G. Amare, G. Alemu, and T. Gashaw, "Spatiotemporal variability and trends of rainfall and its association with Pacific ocean sea surface temperature in west harerge zone, eastern Ethiopia," *Environmental Systems Research*, vol. 10, no. 1, Article ID 7, 2021.

[45] E. Meresa and G. Taye, "Estimation of groundwater recharge using GIS-based wetspass model for birki watershed, the eastern zone of tigray, northern Ethiopia," *Sustainable Water Resources Management*, vol. 5, pp. 1555–1566, 2019.

[46] J. Panthi, P. Dahal, M. Shrestha et al., "Spatial and temporal variability of rainfall in the Gandaki river basin of Nepal Himalaya," *Climate*, vol. 3, no. 1, pp. 210–226, 2015.

[47] K. C. Abbaspour, E. Rouholahnejad, S. Vaghefi, R. Srinivasan, H. Yang, and B. Kløve, "A continental-scale hydrology and water quality model for Europe: calibration and uncertainty of a high-resolution large-scale SWAT model," *Journal of Hydrology*, vol. 524, pp. 733–752, 2015.

[48] D. N. Moriasi, M. W. Gitau, N. Pai, and P. Daggupati, "Hydrologic and water quality models: performance measures and evaluation criteria," *Transactions of the ASABE*, vol. 58, no. 6, pp. 1763–1785, 2015.

[49] T. A. Tesema and O. T. Leta, "Sediment yield estimation and effect of management options on sediment yield of Kesem dam watershed, awash basin, Ethiopia," *Scientific African*, vol. 9, Article ID e00425, 2020.

[50] H. Xie, L. Longuevergne, C. Ringler, and B. R. Scanlon, "Calibration and evaluation of a semi-distributed watershed model of sub-Saharan Africa using GRACE data, hydrol," *Hydrology and Earth System Sciences*, vol. 16, no. 9, pp. 3083–3099, 2012.

[51] D. Sun, H. Yang, D. Guan et al., "The effects of land use change on soil infiltration capacity in China: a meta-analysis," *Science of The Total Environment*, vol. 626, pp. 1394–1401, 2018.

[52] C. Seong, V. Sridhar, and M. M. Billah, "Implications of potential evapotranspiration methods for streamflow estimations under changing climatic conditions," *International Journal of Climatology*, vol. 38, no. 2, pp. 896–914, 2018.